

# High-Spectral-Efficiency Optical Modulation Formats

Peter J. Winzer

(Invited Paper)

**Abstract**—As 100-Gb/s coherent systems based on polarization-division multiplexed quadrature phase shift keying (PDM-QPSK), with aggregate wavelength-division multiplexed (WDM) capacities close to 10 Tb/s, are getting widely deployed, the use of high-spectral-efficiency quadrature amplitude modulation (QAM) to increase both per-channel interface rates and aggregate WDM capacities is the next evolutionary step. In this paper we review high-spectral-efficiency optical modulation formats for use in digital coherent systems. We look at fundamental as well as at technological scaling trends and highlight important trade-offs pertaining to the design and performance of coherent higher-order QAM transponders.

**Index Terms**—Coding, coherent detection, digital signal processing, DSP, FEC, modulation, PDM, QAM, QPSK, SDM, WDM.

## I. INTRODUCTION

THE amount of traffic carried on backbone networks has been growing exponentially over the past two decades, at about 30 to 60% per year (i.e., between 1.1 and 2 dB per year<sup>1</sup>), depending on the nature and penetration of services offered by various network operators in different geographic regions [1], [2]. The increasing number of applications relying on machine-to-machine traffic and cloud computing could accelerate this growth to levels typical within data-centers and high-performance computers [3], [4]: According to Amdahl's rule of thumb [5], [6], the interface bandwidth of a balanced computer architecture is proportional to its processing power. Since cloud services are increasingly letting the network take the role of a distributed computer interface, the required network bandwidth for such applications may scale with data processing capabilities, at close to 90% (or 2.8 dB) per year [7]. Non-cacheable real-time multi-media applications will also drive the need for more network bandwidth.

For over two decades, the demand for communication bandwidth has been economically met by wavelength-division multiplexed (WDM) optical transmission systems, researched,

developed, and abundantly deployed since the early 1990s [8]. Fig. 1(a) illustrates the evolution of single-channel bit rates (single-carrier, single-polarization, electronically multiplexed; circles), as well as of aggregate per-fiber capacities using wavelength-, polarization-, and most recently space-division multiplexing (WDM, PDM, SDM; triangles), as achieved in various record research experiments; commercial products follow similar trends, with a time delay of typically 5 years [1], [8], [9].

As can be seen from Fig. 1(a), WDM was able to boost the relatively slow progress in single-channel bit rates (at 0.5 dB/year) to 2.5 dB/year during the 1990s, which was more than enough to satisfy the 2-dB/year traffic growth and partly contributed to the telecom bubble around 2000 [1]. Technologically, the steep initial growth of WDM capacities reflects rapid advances in optical, electronic, and optoelectronic device technologies, such as wide-band optical amplifiers, frequency-stable lasers, and narrow-band optical filtering components. By the early 2000s, lasers had reached Gigahertz frequency stabilities, optical filters had bandwidths allowing for 50-GHz WDM channel spacings, and electronically generated and directly detected 40-Gb/s binary optical signals started to fill these frequency slots. At this remarkable point in time where “optical and electronic bandwidths had met,” optical communications had to shift from physics toward communications engineering to further increase *spectral efficiencies*, i.e., to pack more information into the limited ( $\sim 5$ -THz) bandwidth of the commercially most attractive class of single-band (C- or L-band) optical amplifiers. Consequently, by 2002 high-speed fiber-optic systems research had started to investigate binary [10] and quaternary [11] phase shift keying (BPSK, QPSK) using direct detection with differential demodulation (DPSK, DQPSK) [12], [13], followed by commercial deployment at 40 Gb/s [14], [15]. With the drive towards per-channel bit rates of 100 Gb/s in 2005 [16], however, it became clear that additional techniques were needed if 100-Gb/s channels were to be used on the by then widely established 50-GHz WDM infrastructure, supporting a spectral efficiency of 2 b/s/Hz [17], [18]. In this context, polarization-division multiplexed (PDM) QPSK allowed for a reduction of symbol rates by a factor of 4 compared to the information bit rate, which brought 40 and 100-Gb/s optical signals at around 10 and 25 GBaud within the reach of fast analog-to-digital converters (ADCs). This, in turn, enabled the use of digital coherent detection using robust digital signal processing (DSP) to perform all-electronic chromatic- and polarization-mode dispersion compensation,

Manuscript received June 12, 2012; revised August 02, 2012; accepted August 02, 2012. Date of publication August 23, 2012; date of current version December 12, 2012.

The author is with Bell Labs, Alcatel-Lucent, Holmdel, NJ 07733 USA (e-mail: peter.winzer@bell-labs.com).

Color versions of one or more of the figures in this paper are available online at <http://ieeexplore.ieee.org>.

Digital Object Identifier 10.1109/JLT.2012.2212180

<sup>1</sup>Following [1], we conveniently express traffic growth in decibels, i.e., a 30% growth corresponds to a growth of  $10 \log_{10}(1.3) = 1.14$  dB.

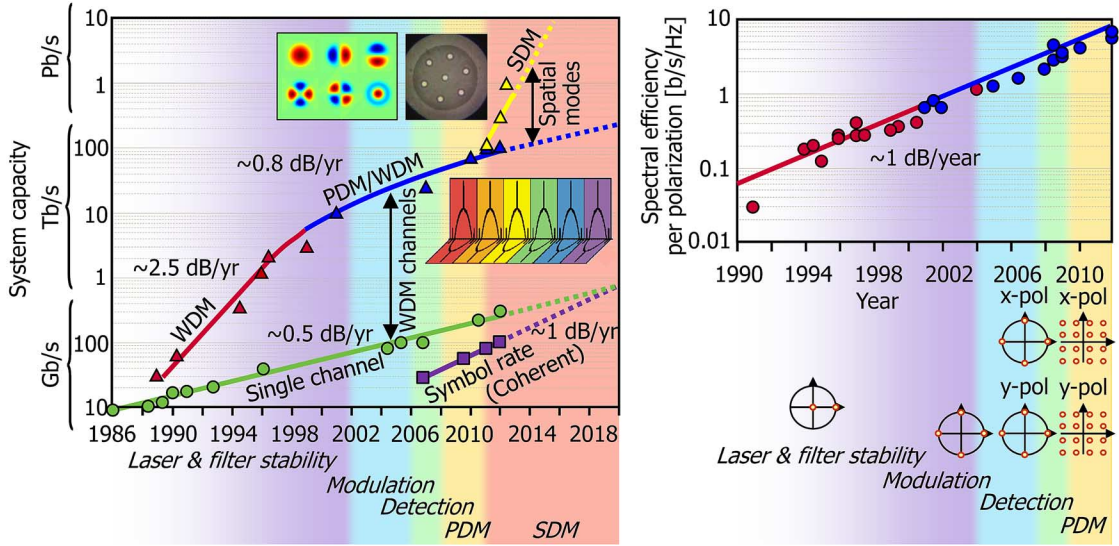


Fig. 1. (a) Evolution of experimentally achieved *single-channel bit rates* (single-carrier, single-polarization, electronically multiplexed; green circles), *symbol rates* in digital coherent detection (purple squares), and *aggregate per-fiber capacities* (triangles) using wavelength-division multiplexing (WDM; red), polarization-division multiplexing (PDM; blue), and space-division multiplexing (SDM; yellow). (b) Evolution of experimentally achieved *per-polarization spectral efficiencies* in single- (red) and dual-polarization (blue) experiments.

frequency- and phase locking, and polarization demultiplexing [19]–[26]. Commercial coherent systems for fiber-optic networks were introduced at 40 and 100 Gb/s in 2008 and 2010, using PDM-QPSK at 11.5 and 28 GBaud, based on custom-designed CMOS ASICs to handle the massive DSP functionality [27], [9].

The adoption of advanced coherent communication concepts widely used in radio-frequency systems allowed spectral efficiencies to continue their scaling at  $\sim 1$  dB/year using essentially unchanged optical line systems, cf. Fig. 1(b). Reduced to this growth rate, however, WDM capacity growth slowed down to  $\sim 0.8$  dB/year, and is expected to slow down even further as systems are rapidly approaching the nonlinear Shannon limit of the fiber-optic channel [28]. In 2011, space-division multiplexing (SDM) research experiments using multi-core fiber started to beat single-mode aggregate per-fiber capacities [29], [30], [112], promising to restore the aggregate per-fiber capacity growth, as shown in Fig. 1(a).

In this paper, we discuss higher-order coherent optical modulation formats as the underlying technology that has fueled capacity growth over the past  $\sim 5$  years. In Section II, we review, on an intuitive and basic level, the notions of symbol constellation, pulse shaping, multiplexing, and coding, which are key to advanced transponder and systems design. We then apply these concepts in Section III to illustrate important fundamental and technological trade-offs that have to be made when choosing a modulation format. We show that these trade-offs depend on whether utmost per-channel interface rates, WDM capacities, or transmission reach are desired.

## II. THE ANATOMY OF A MODULATION FORMAT

### A. Digital Communications and the Structure of Language

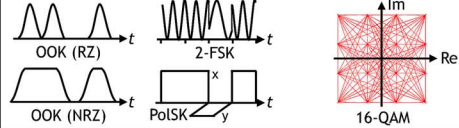
The basic structure of digital communication signals (optical and electronic alike) resembles the structure of many languages

in several ways [31], as illustrated in the left column of Table I [32]. A finite set (or *alphabet*) of letters is used to form words and sentences, whereby letters are written in series, one after the other. The countably discrete nature of letters contained in a (language-specific) alphabet motivates the term digital<sup>2</sup>. Note that letters are abstract concepts that need to be mapped into the physical reality of the analog world we live in. This is done by representing each letter by some kind of *analog waveform* that bears key features of the letter. For example, the letter ‘A’ in the 26-ary Latin alphabet can be represented by the analog waveforms **A**, *A*, **а**, *А*, **À**, etc. As long as writer (transmitter) and reader (receiver) use the same alphabet and are able to establish the correct mapping between the analog waveforms and the set of letters, communication may take place.

On top of using a well-defined alphabet of letters, each language also uses a considerable amount of *redundancy*. This is done by forming words and sentences from letters. By allowing a much smaller number of words and sentences than what would be mathematically possible by arbitrarily arranging letters within words and words within sentences, the receiver is put in the position to correct for spelling errors. For example, the words ‘langua’ or ‘langya’ are immediately identified as misspelled versions of the correct code word ‘language’. Being able to *identify* and *correct* these typos shows the ability of our brain to act as an efficient error correction device. Language redundancy in the form of synonyms can also be employed by the transmitter to avoid the use of certain words that are known to cause trouble in conveying a message. For example, many non-native English speakers mispronounce a ‘th’ as an ‘s,’ which can lead to uncorrectable confusion if both resulting words are legitimate English words, such as the words ‘think’ and ‘sink’. Error correction may still be possible on a sentence level by identifying a word’s most likely meaning within a given

<sup>2</sup>The word digital is derived from the Latin word “digitus” (finger) and alludes to the basic way of counting members of discrete sets.

TABLE I  
THE STRUCTURE OF DIGITAL COMMUNICATIONS IN MANY WAYS RESEMBLES THE STRUCTURE OF LANGUAGE [31], [32]

Language	Digital communications
Alphabets of letters {A,B,C,...,Z}, {α,β,γ,...,ω}, {0,1,2,...,9}	Symbol alphabets (constellations)  Binary one-dimensional    Binary orthogonal    Quaternary    16-ary
Analog letter representations 'A' → <b>A</b> , <b>Ā</b> , <b>ā</b> , <b>Ä</b> , <b>Ǻ</b> , ...	Analog waveform representations  OOK (RZ)    2-FSK    OOK (NRZ)    PoFSK    16-QAM
Letters arranged in series	One symbol transmitted per symbol period
Redundancy in words or sentences 'lague' or 'language' → 'language'	Error correcting codes Overhead in time (forward error correction, FEC) or in symbol alphabet (coded modulation)
Synonym expressions (ex: use 'ponder' instead of 'think' to avoid confusion with 'sink')	Line coding Overhead in time or in symbol alphabet (ex: '11011' → {+1,+1,0,-1,-1}: 'Duobinary')

context, but this kind of error correction is much more prone to mistakes than the one on the individual word level. It may thus prove advantageous to substitute words containing 'th' by suitable synonyms to *avoid* likely errors in the first place rather than having to correct for them after they have occurred.

### B. Digital Symbol Constellations and Analog Pulse Shapes

The above outline of basic language structure illustrates many important concepts used in advanced digital communication systems, as summarized in the right column of Table I. In digital communications, the alphabet of letters becomes an alphabet (also called a *constellation*) of discrete communication symbols  $\{a_k\}$ . Importantly, these symbols can be viewed as an abstraction that does not yet assign physical meaning. Before transmitting symbols over a physical channel, a set of *analog waveforms*  $x_k(t)$  has to be chosen to map an abstract symbol constellation onto physical reality. Once mapped to analog waveform representations, the symbols are sequentially transmitted at rate  $R_S$ , one symbol per symbol period  $T_S = 1/R_S$ , resulting in the transmit waveform

$$s(t) = \sum_k x_k(t - kT_S). \quad (1)$$

The symbol rate  $R_S$  is measured in 'baud,' where 1 baud = 1 symbol/s. If all symbols in an  $M$ -ary alphabet (i.e., an alphabet of  $M$  letters) occur with equal probability, and if all symbols carry user information, each symbol conveys  $\log_2 M$  bits of information, and bit rate  $R_B$  and symbol rate  $R_S$  are related by

$$R_B = R_S \log_2 M. \quad (2)$$

For example, the simple binary symbol constellation shown first in Table I consists of two symbols, each conveying one bit of information. The key feature of these two letters is that one of them carries no energy and one of them does carry energy (as measured by their distance from the origin in the symbol constellation). One may then choose to represent the

two symbols by 'sending no pulse' and 'sending a pulse,' respectively. The exact shape of the pulse adds detail to the format and its transmission performance over the analog channel, just as **A**, **Ā**, **ā**, **Ä**, **Ǻ** show key similarities but differ in their details. This simplest of all modulation formats is called on/off keying (OOK) and is still the almost exclusively deployed format at per-channel bit rates up to 10 Gb/s.

Another example is the binary orthogonal alphabet shown second in Table I. The key feature of this alphabet is that the two letters are *orthogonal* (in whatever physical dimension) and that both letters have equal energy. In general, two analog waveforms  $\vec{x}_1(t, \vec{r})$  and  $\vec{x}_2(t, \vec{r})$  representing complex spatial optical field distributions are orthogonal if their inner product vanishes [33], [34], i.e., if <sup>3</sup>

$$\int_{-\infty}^{\infty} dt \iint_{-\infty}^{\infty} d\vec{r} \vec{x}_1(t, \vec{r}) \cdot \vec{x}_2^*(t, \vec{r}) = 0 \quad (3a)$$

$$\int_{-\infty}^{\infty} df \iint_{-\infty}^{\infty} d\vec{r} \vec{X}_1(f, \vec{r}) \cdot \vec{X}_2^*(f, \vec{r}) = 0 \quad (3b)$$

where  $t, f$ , and  $\vec{r}$  denote time, frequency, and the transversal spatial coordinates respectively, and  $X(f) = \mathcal{F}\{x(t)\}$  is the Fourier transform of  $x(t)$ . Important examples for (scalar) orthogonal waveforms in time and frequency domain are shown in Fig. 2. In particular, waveforms that are *non-overlapping* either in time (cf. (3a)) or in frequency (cf. (3b)) are orthogonal, irrespective of their shape. Further,  $T_S$ -time-shifted copies of certain temporally *overlapping* pulses  $x(t)$  are orthogonal if  $\mathcal{F}^{-1}\{|X(f)|^2\}$  has nulls at integer multiples of  $T_S$ , which follows from (3b) with  $X_2(f) = X_1(f) \exp(j2\pi f k T_S)$ . This condition is equivalent to Nyquist's criterion for no inter-symbol

<sup>3</sup>Regarding *spatial* orthogonality, the overlap integrals in (3) are an approximation of a more general orthogonality condition involving the  $z$ -component of the propagating electromagnetic field [35].

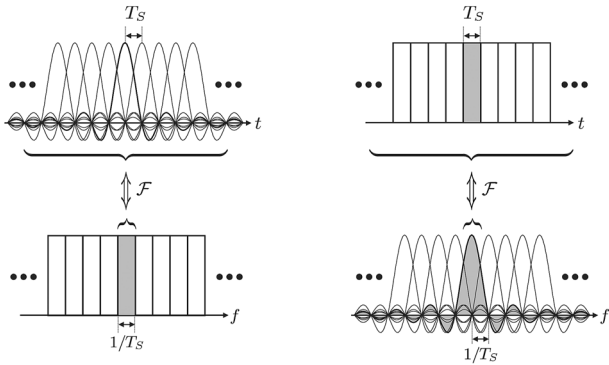


Fig. 2. Examples for waveform orthogonality in time and frequency.

interference (ISI) [33]. An important class of pulse shapes satisfying this criterion are square-root raised cosine pulses [33]. By the same token,  $R_S$ -frequency-shifted copies of  $X(f)$  are orthogonal provided that  $\mathcal{F}\{|x(t)|^2\}$  has nulls at integer multiples of  $R_S = 1/T_S$ , as illustrated in Fig. 2. This condition is at the heart of pulse shaping in orthogonal frequency division multiplexing (OFDM) [36].

To transmit the binary orthogonal alphabet of Table I, one could choose to map each letter onto (any) one of two orthogonal polarizations (polarization-shift keying, PolSK), one of two orthogonal frequencies (frequency-shift keying, FSK), one of two orthogonal time slots (pulse position modulation, PPM), or one of two orthogonal spatial modes (mode-orthogonal modulation). Obviously, a receiver built to detect PolSK will be unable to detect FSK, and vice versa. This underlines the importance of properly specifying *both* the symbol alphabet *and* the set of corresponding analog physical waveform representations to make digital communications work.

An important set of orthogonal physical dimensions that can be used to construct two-dimensional symbol alphabets in digital communications is the *quadrature space*, composed of real and imaginary components of a bandpass signal (also called ‘sine’ and ‘cosine’ or in-phase (I) and quadrature (Q) components). For example, the quaternary (4-ary) or the 16-ary alphabets shown in Table I are usually mapped onto real and imaginary parts of the complex optical field, where they are then called quaternary (or ‘quadrature’) phase-shift keying (QPSK) and 16-ary quadrature amplitude modulation (16-QAM), respectively. Table I visualizes one of many possible mappings of 16-QAM to physical waveforms; here, the analog waveform transitions along straight lines within the complex plane of the optical field. QAM signals typically use the same analog pulse shape for all symbols in the constellation, i.e.,  $x_k(t) = x(t)$ , which lets the transmitted waveform take the form

$$s(t) = \sum_k a_k x(t - kT_S). \quad (4)$$

Constellations in more than two dimensions can also be constructed, e.g., by using  $M$  orthogonal time slots ( $M$ -PPM) or  $M$  orthogonal frequencies ( $M$ -FSK) to improve sensitivity at the expense of spectral efficiency [33]. Higher-dimensional spaces can also be constructed by combining different physical dimensions. Recent examples include polarization-switched QPSK (PS-QPSK), combining quadrature and polarization to

construct a 4-dimensional signal constellation for high sensitivity at high spectral efficiency [37], [38], or a combination of PPM and PDM-QPSK for highest sensitivities at reduced bandwidth expansion compared to a pure PPM or FSK approach [39].

### C. Multiplexing

If information is transmitted on  $p$  parallel channels, the aggregate bit rate of the resulting *multiplex* is given by the single-channel bit rate multiplied by the number of parallel channels,

$$R_B = pR_S \log_2 M. \quad (5)$$

Parallel channels can be established using the  $x$  and  $y$  polarization of the optical field ( $p = 2$ ),  $p$  orthogonal frequencies, or  $p$  orthogonal spatial modes [34]. In optical communications, frequency-division multiplexing (FDM) comprises WDM as well as optical superchannels and OFDM with  $p$  orthogonal yet spectrally overlapping subcarriers [40]. Fig. 2 visualizes two important examples for the use of orthogonal subcarriers to form Nyquist WDM (left) and OFDM (right). Importantly, the characteristics of a modulation format are largely independent of the multiplexing strategy. In particular, and certain implementation aspects aside, OFDM, optical superchannels, and single-carrier systems based on the same modulation format achieve the same spectral efficiency and exhibit the same tolerance to noise and other linear signal impairments; the tolerance to *nonlinear* signal distortions is approximately the same for typical dispersion uncompensated system parameters [41]–[43].

### D. Coding

Returning to our structural comparison in Table I, as with language, redundancy in digital communications can be introduced either to *avoid* certain symbol combinations that are known to cause trouble on a specific communication channel (*line coding*) or to *correct* errors at the receiver (*forward error correction*, FEC). Both techniques may introduce the required overhead in a variety of ways. The most common physical dimensions to include coding overhead are the time domain (by transmitting at a higher symbol rate than what would be required by the client application), and the symbol constellation (by adding additional symbols to carry redundancy as opposed to user information). The gross channel bit rate, including all coding redundancy, is usually referred to as the *line rate*.

An important quantity associated with codes is the code rate<sup>4</sup>  $R_c \leq 1$ , defined as the ratio of information bit rate to line rate. In optical communications, the term *coding overhead* (OH), i.e., the percentage of bits that are added to the information bits for coding redundancy, is more commonly used. Coding overhead and code rate are related by [28]

$$\text{OH} = (1 - R_c)/R_c. \quad (6)$$

Overheads around 7% have been standard for fiber-optic communication systems for about a decade [44], and soft-decision FECs with overheads around 20% are being developed for next-generation systems [45], [46].

<sup>4</sup>Note that the code rate is a dimensionless quantity as opposed to a bit rate or a symbol rate, which carry units of ‘per second’.

If overhead is added solely in the time domain, maintaining a given information bit rate requires transmission at a proportionally higher symbol rate, which can lead to increased implementation penalties due to band-limited transmitter and receiver hardware. Furthermore, higher-bandwidth signals passing through multiple reconfigurable optical add/drop multiplexers (ROADMs) in an optically routed network may experience more severe filter-induced spectral narrowing. Obviously, for a code to prove in, all penalties arising from an increased symbol rate must be compensated for by the code's performance improvement, which leads to the notion of an application-specific *net coding gain*. A way to avoid increased symbol rates for increased FEC OH is to put redundancy into the symbol constellation itself, by adding more symbols than required for information transport at a target spectral efficiency. This technique (sometimes referred to as 'coded modulation' [47]) is well studied in electronic and wireless communications and is starting to enter optical communications as well [28], [48]–[52]. We will discuss this technique further in the context of Fig. 6(b).

For more details on the basics of digital communications and coding, the interested reader is referred to classic textbooks such as [33], [53]–[55]. Detailed tutorials on the basics of digital *optical* communications can be found in, e.g., [13], [28], [34]. Recent reviews specific to optical communications include [9], [12], [13], [28], [32], [56]–[58].

### III. KEY TRADE-OFFS IN CHOOSING A MODULATION FORMAT

The question as to the 'best' optical modulation format is frequently encountered in optical transmission system design. As might be expected, there is no unique answer to this question. Rather, the answer depends on system requirements such as:

- Target per-channel interface rate
- Available per-channel optical bandwidth
- Target WDM capacity (or spectral efficiency)
- Target transmission reach
- Optical networking requirements
- Transponder integration and power consumption

Each of the above boundary conditions implies a certain set of trade-offs that help to determine the 'best' modulation format. In this section, we highlight some of the key trade-offs impacting the selection of a modulation format for specific applications.

#### A. Symbol Rate versus Constellation Size—DAC Resolution

In order to increase *per-channel interface rates* (cf. green circles in Fig. 1), one can increase the symbol rate  $R_S$ , the constellation size  $M$ , or the multiplexing factor  $p$ . According to (5), the resulting speed improvement is linear in  $R_S$  and  $p$  but only logarithmic in  $M$ . As a consequence, increasing line rates by means of larger symbol constellations becomes progressively harder as  $M$  is increased. Fig. 3 visualizes this situation, showing experimentally achieved combinations of symbol rates (single-carrier-equivalent symbol rates for OFDM) and bits per symbol,  $\log_2 M$ . Red squares denote transmitters employing digital pulse shaping or OFDM, while blue circles represent transmitters whose pulse shapes  $x(t)$  are inherently determined by the characteristics of the transmit electronics and

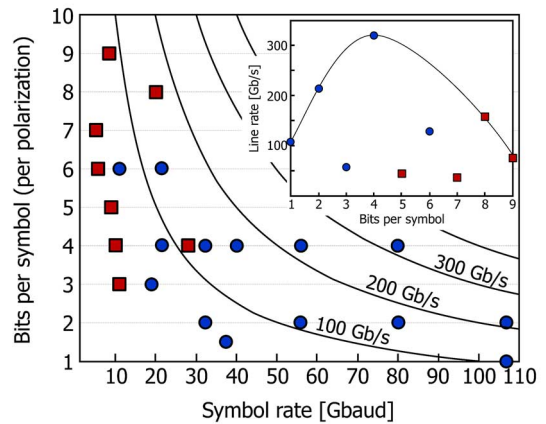


Fig. 3. Summary of single-channel (single carrier, single polarization, electronically multiplexed) higher-order modulation experiments and contours of constant single-channel line rates. *Inset*: Maximum achieved single-channel line rate versus constellation size. (Red squares: Digital pulse shaping or OFDM. Blue circles: No digital pulse shaping.)

optics. (The role of digital pulse shaping in optical transmission systems is further discussed in Section III.F.) Contours of constant single-channel (single carrier, single polarization, electronically multiplexed) line rates are also shown. The inset gives the maximum single-channel line rate achieved in research experiments at a particular number of bits per symbol. Interestingly, the speed trade-off between  $R_S$  and  $M$  settles at  $M = 16$ , revealing 16-QAM as the modulation format that has so far allowed for the highest single-channel interface rate of 320 Gb/s at 80 Gbaud, polarization multiplexed to a single-carrier 640-Gb/s [59].

To generate a square  $M$ -QAM constellation using a single I/Q modulator (driven by two quadrature signals with  $\sqrt{M}$  amplitude levels), one needs two digital-to-analog converters (DACs), each with a minimum resolution of  $\log_2 \sqrt{M}$  bits, at a sampling rate equal to the symbol rate. Having higher-resolution DACs allows for compensation of modulator or driver nonlinearities [60]; having over-sampled DACs further allows for digital pulse shaping and OFDM, as discussed in Section III.F. Commercial DACs built in CMOS technology are currently available up to 65 GSamples/s with as much as 8-bit resolution [61], capable of producing constellations beyond 16-QAM. Compared to the inset of Fig. 3, this could shift the optimum constellation size in terms of raw interface rates to  $M > 16$  for CMOS-integrated DAC+DSP ASIC solutions. The state-of-the-art in high-speed DAC technologies is further reviewed in [62], [63].

In order to go beyond technologically achievable *single-channel* line rates using the best trade-off between  $R_S$  and  $M$  requires *multiplexing* in the polarization, frequency, or spatial dimension, as discussed in Section II.C. For example,  $p = 12$  spatial paths have been used for low-power  $\sim 100$ -Gb/s short-reach interfaces [3], and optical superchannels with, e.g.,  $p = 24$  orthogonal optical subcarriers have been used to achieve aggregate line rates of 1.2 Tb/s, transmitted over long-haul (7200-km) distances [40], [64]. All parallel approaches used to scale interface rates ask for photonic integration in order to be economically viable [3], [65], [66].

TABLE II  
APPROXIMATE ENOB REQUIREMENTS FOR ADCs  
USED FOR DIGITAL COHERENT QAM DETECTION

$M$	$\log_2(M)$	$\sqrt{M}$	$\log_2(\sqrt{M})$	ENoB [67]
4	2	2	1	~4
16	4	4	2	~5
64	6	8	3	~6
256	8	16	4	~7

### B. Symbol Rate versus Constellation Size—ADC Resolution

Related to the resolution of the transmit-side DAC is that of the receive-side ADC, usually specified in terms of its effective number of bits<sup>5</sup> (ENoB). As shown in [67], the required ADC resolution at a 1-dB receiver sensitivity penalty and at a pre-FEC bit error ratio (BER) typical of coded systems (e.g.,  $10^{-3}$ ) is approximately 3 bits more than what would be needed to recover the  $\sqrt{M}$  amplitude levels of the two signal quadratures if the constellation were received without any distortions and phase rotations (cf. Table II).

The technological trade-off between ADC resolution and bandwidth is analyzed in a series of papers by Walden [68], [69], and reveals a reduction of about 3.3 ENoB per decade of analog input bandwidth. This reduction of available ENoB with detection bandwidth is also frequently observed in optical superchannel experiments [40]: The detection of a single optical subcarrier (isolated by optical or analog electronic filtering *prior* to digitization) typically shows better performance than the simultaneous detection of multiple subcarriers followed by digital filtering after the ADC. The reason for this observation is that in the latter case the amplitude resolution of the ADC is shared among *all* detected subcarriers, which accordingly reduces the ENoB available for *each individual* subcarrier.

According to Walden's studies, converters improve at a rate of  $\sim 1/3$  ENoB per year at fixed bandwidth, or at 27% (1 dB) per year in bandwidth at fixed ENoB, which matches the evolution of symbol rates in digital coherent detection experiments, represented by purple squares in Fig. 1(a). Commercial CMOS based ADCs achieve up to 65 GSamples/s at close to 6 ENoB across a  $\sim 20$ -GHz bandwidth [61], [70]. Using 28-nm CMOS technology, ADC bandwidths of  $\sim 30$  GHz at sampling rates between 80 and 100 GSamples/s at  $\sim 6$  ENoB are expected to be available soon [71]. The state-of-the-art in high-speed ADC technologies is further reviewed in [62], [63].

Looking at the speed versus converter resolution trade-off in terms of a combined transmitter/receiver sensitivity penalty, Fig. 4 displays back-to-back implementation penalties (i.e., the gap between experimentally achieved and theoretically possible signal-to-noise ratios at a reference BER of  $10^{-2}$ ) for recent research experiments. The black curves are contours of constant single-channel (single carrier, single polarization) line rates, as in Fig. 3. The gray lines represent a linear least-squares fit to the reported experimental implementation penalties, revealing a slope close to 4 bits/decade. Within reasonable limits reflecting the significant scatter of the penalty data, this suggests that it is 'equally hard' to build, e.g., an 8-GBaud 256-QAM system [72]

<sup>5</sup>Although ENoB is the most commonly used performance metric for high-speed DACs and ADCs, a clear relationship between ENoB and the BER performance of a digital coherent receiver has not yet been established.

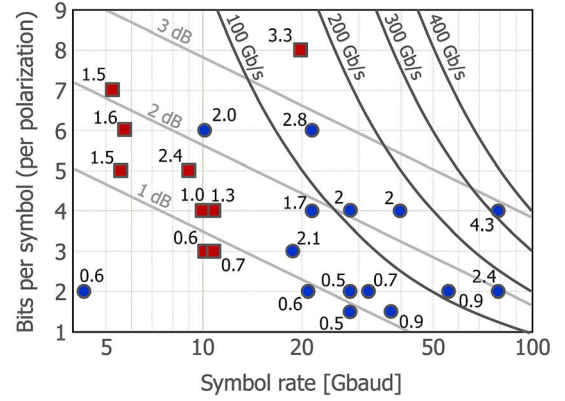


Fig. 4. Summary of experimentally achieved implementation penalties at BER =  $10^{-2}$  for single-channel (single carrier, single polarization, electronically multiplexed) higher-order modulation formats. Gray lines represent a linear fit to the penalty data, revealing a slope of 3.9 bits/symbol per decade of symbol rate. Black lines represent contours of constant single-channel line rates. (Red squares: Digital pulse shaping or OFDM. Blue circles: No digital pulse shaping.)

as it is to build an 80-GBaud 16-QAM system [59], at least in a research context.

### C. Symbol Rate versus Constellation Size—Digital Filter Sizes

Since digital coherent receivers have the entire optical field information available in digital form, linear optical impairments can be readily compensated for by digital filters within the receiver's DSP. The most important such impairments are chromatic dispersion (CD), polarization-mode dispersion (PMD), and filtering impairments as they arise from a signal's multiple passes through ROADMs in an optically routed network. Today's DSP ASICs are capable of handling the CD of more than 2000 km of standard single-mode fiber (SSMF, 17 ps/km nm), equivalent to a CD compensation capability of  $\sim 34$  ns/nm, at  $\sim 30$  GBaud [73].

Chromatic dispersion represents an all-pass filter with quadratic phase [74], which can be compensated using a filter with the inverse phase profile [75]. The length of such a filter's impulse response (in terms of  $T_S/2$  spaced filter taps) is approximately given by  $0.032 \cdot CD_{[\text{ns/nm}]} \cdot R_S^2_{[\text{GBaud}]}$  [75], which amounts to  $\sim 1000$  taps for the above parameters. As adjacent-pulse overlap due to dispersive pulse broadening scales quadratically with symbol rate, doubling  $R_S$  results in a quadrupled number of filter taps to compensate for the same fiber length's worth of CD; other linear impairments such as PMD or concatenated filtering scale linear with symbol rate. On the other hand, keeping the symbol rate fixed and scaling the transponder's interface rate by going to higher-order constellations keeps the required filter lengths unchanged (but may limit the reach due other factors discussed in this section).

### D. Symbol Rate versus Constellation Size—Laser Phase Noise

In addition to the above considerations, the trade-off between symbol rate and constellation size is also impacted by *phase noise*. Random phase fluctuations of signal and/or local oscillator (LO) light as well as pattern-dependent phase perturbations induced by fiber nonlinearities [76] translate into angular noise that ultimately degrades detection performance. The tolerance

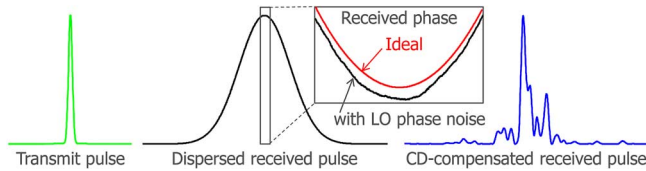


Fig. 5. Local oscillator phase noise induced pulse distortions from digital coherent detection.

to phase noise depends substantially on the underlying detection algorithm and its hardware implementation [67], [77], [78]. In general, higher-order modulation formats become progressively more sensitive to phase noise. Since it is the phase noise accumulation across a modulation symbol (or multiples thereof) that determines the impact of phase noise on detection performance, the tolerance to laser phase noise for a given detection algorithm and modulation format depends on the ratio of the combined signal and LO laser linewidth  $\Delta\nu_{\Sigma}$  to the symbol rate,  $\Delta\nu_{\Sigma}/R_S$  (or, equivalently, on the product of laser linewidth and symbol duration,  $\Delta\nu_{\Sigma}T_S$ ). For small ( $\sim 0.5$ -dB) penalties and at typical pre-FEC BERs between  $10^{-2}$  and  $10^{-3}$ , QPSK tolerates values of  $\Delta\nu_{\Sigma}T_S$  on the order of  $10^{-4}$ , 16-QAM on the order of  $10^{-5}$ , and 64-QAM on the order of  $10^{-6}$  [67], [77], [79]. Hence, a  $\sim 100$ -kHz linewidth external cavity laser (ECL) is an appropriate light source down to symbol rates of several GBaud for QPSK and down to  $\sim 10$  GBaud for 16-QAM. Significantly higher-order constellations at  $\sim 10$  GBaud or below require narrower-linewidth lasers [72] or particularly phase-noise tolerant DSP algorithms [80] to avoid sensitivity penalties from laser phase noise. On the other hand, going to higher symbol rates proportionally relaxes laser phase noise requirements. For example, 64-QAM at 21.4 GBaud has been demonstrated using a  $\sim 100$ -kHz ECL [81], 16-QAM at 14 GBaud has been shown to tolerate  $\sim 1$  MHz of laser linewidth [82], and QPSK at  $\sim 100$  GBaud was demonstrated using linewidths of about 10 MHz, which allowed for distributed feedback (DFB) lasers at negligible phase noise penalties [83].

Another important aspect related to laser phase noise in digital coherent receivers is the conversion of laser phase noise to intensity noise within the CD filter [84], [85]. This effect can also be understood as signal decoherence induced by LO phase noise, as visualized in Fig. 5: The fiber's CD spreads the signal (together with all the *signal* laser's phase fluctuations) over a large number of symbols ( $\sim 500$  for a 2000-km SSMF link at 30 GBaud). An ideal digital coherent receiver compensates for this temporal spreading by applying the inverse CD in the digital domain, where the digital CD compensation filter restores the transmit signal by coherently superimposing the dispersed received signal components within a range of, e.g.,  $\pm 250$  symbols. However, if the phase of these samples exhibits random fluctuations (generated by the LO laser's phase noise, cf. Fig. 5), far-apart samples of the received signal that need to be superimposed by the CD compensation filter are no longer coherent, which inevitably degrades the digital superposition process. As a consequence, high-speed signals become *less* tolerant to LO laser phase noise in the presence of long digital filters such as needed for significant CD compensation. For example, [85] shows that the LO laser linewidth tolerance for PDM-QPSK at

a 0.5-dB sensitivity penalty and for a CD compensation capability of 30 ns/nm ( $\sim 1800$ -km SSMF) drops from 3 MHz to less than 500 kHz (instead of increasing to 16 MHz) when going from 10.7 GBaud to 56 GBaud. Experiments at 107 GBaud confirm this observation [83]. This trade-off suggests an optimum symbol rate with respect to laser phase noise in digitally CD compensated coherent systems.

### E. Spectral Efficiency versus Noise and Transmission Reach

While our above considerations were all linked to trade-offs involving per-channel interface rates, one of the most important trade-offs in advanced system design is largely *independent* of single-channel interface rates or the number of sub-carriers in an OFDM or optical superchannel multiplex. This independence is exact in the linear regime and in the presence of fiber nonlinearities is approximately valid for typical dispersion uncompensated system parameters [41]–[43]: The trade-off between *spectral efficiency* and *system reach* depends predominantly on the underlying modulation format and FEC, and determines the maximum WDM capacity that can be transmitted over a given distance within a practical optical amplification bandwidth. Fig. 6(a) visualizes this trade-off in the linear regime, showing the achievable (single-polarization) spectral efficiency as a function of the received SNR per bit [28], [33]. The Shannon limit for a linear, additive white Gaussian noise channel [31] is shown together with the theoretical performance of various higher-order square QAM constellations (blue circles) assuming Gray-coded symbol mapping and state-of-the-art 7% overhead hard-decision FEC capable of correcting an input BER of  $3.8 \cdot 10^{-3}$  to values below  $10^{-15}$  [44]. Representative experiments are denoted by red squares. Performance will shift towards the Shannon limit as more advanced coding [45], [46] and/or non-square QAM constellation shaping [47], [86] are being used. The impact of advanced coding on (linear) system performance is quantified in Fig. 6(b), where the blue circles represent the performance of the 7% hard-decision FEC underlying Fig. 6(a) and the Shannon bounds for the respective square QAM formats with ideal soft-decision FEC are shown as blue curves. The asymptotic gap between square QAM performance and the modulation unconstrained Shannon limit (black curve) amounts to 1.53 dB and can be tapped into by proper constellation shaping, especially for large constellation sizes [47], [86].

Note that the Shannon limit is relatively steep in the low-spectral-efficiency regime but asymptotically flattens out to a slope of 1 b/s/Hz for every 3-dB of higher SNR per bit at high spectral efficiencies. With reference to Fig. 6(a), starting with QPSK as a baseline, doubling system capacity asks for 16-QAM, which comes at the expense of a 3.7-dB higher SNR per bit, or 6.7-dB higher optical SNR (OSNR) [28] at fixed symbol rate, plus a  $\sim 1$ -dB higher expected implementation penalty (cf. Fig. 4). To retain approximately the QPSK transmission reach at 16-QAM, this SNR gap may be closed through techniques such as:

- (i) stronger (soft-decision) FEC or coded modulation [45], [46], [86] to lower the receiver's SNR requirements and move both theoretical and experimental points in Fig. 6(a) closer to their Shannon bounds. In the spirit of coded modulation, as indicated in Fig. 6(b), one may choose

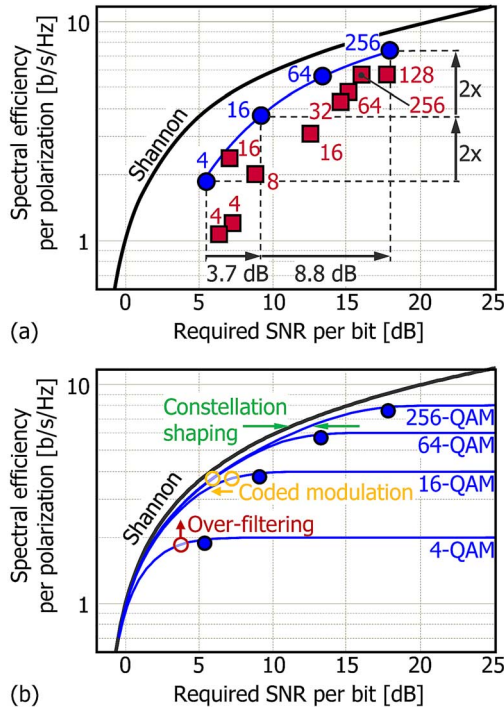


Fig. 6. Dependence of (single-polarization) spectral efficiency on the received SNR per bit. The Shannon limit for a linear, additive white Gaussian noise channel is shown together with the theoretical performance of various square QAM formats (blue circles), assuming Gray-coded symbol mapping and state-of-the-art 7% overhead hard-decision FEC. Also shown in (a) are representative experimental results (red squares); numbers indicate QAM constellation sizes. In (b), the Shannon limits for various square QAM constellations are shown, and the effects of constellation shaping, coded modulation, and signal over-filtering are indicated.

to transmit, e.g., 64-QAM instead of 16-QAM at a fixed spectral efficiency of 3.73 b/s/Hz, thereby increasing the available coding OH from 7% to 60%. Obviously, the increased coding gain has to offset additional implementation penalties for the higher constellation size;  
 (ii) lower-loss fiber or (potentially higher-order) distributed Raman amplification [87] to improve the OSNR delivered to the receiver;  
 (iii) lower-nonlinearity fiber or more powerful, nonlinear distortion compensating DSP to allow for higher optical signal launch powers [28], [88].

A further doubling in capacity, from 16-QAM to 256-QAM, however, comes at the expense of an additional 8.8 dB in SNR per bit (cf. Fig. 6(a)), which is impossible to accommodate without reducing system reach.

The trade-off between spectral efficiency and system reach, including noise, fiber nonlinearities, as well as current technological shortfalls, is further summarized in Fig. 7, showing the PDM spectral efficiency as a function of transmission distance. Record experimental results (circles) are shown together with the nonlinear Shannon limit of [28]. Both curves trace straight lines on a logarithmic scale for the transmission distance  $L$ , since the delivered SNR is inversely proportional to  $L$ , and the spectral efficiency is given by  $\log_2(1 + \text{SNR}) \approx \log_2(\text{SNR}) \sim \log_2(1/L)$  in the high-SNR regime [89], [90]. The ellipse indicates a range into which

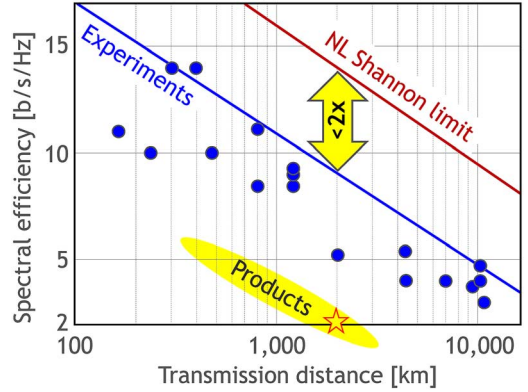


Fig. 7. Trade-off between *dual-polarization* spectral efficiency and transmission reach, showing the nonlinear Shannon limit of [28] together with experimentally achieved results (circles). The ellipse indicates a range into which commercial systems might fall, and the asterisk represents Alcatel-Lucent's commercially deployed optical transmission platform [73].

commercial systems working over installed legacy fiber with appropriate OSNR margins might fall. The asterisk represents Alcatel-Lucent's commercially deployed 1830 optical transmission platform [73]. Importantly, we note that experimental records have approached the nonlinear Shannon limit to within a factor of less than two, which at an annual 2-dB traffic growth rate corresponds to  $\sim 18$  months. Realizing that WDM capacities are no longer scalable, alternative solutions have to be speedily developed. Since shortening the regeneration distance is neither a cost- nor an energy-efficient option [89], the exploitation of space as the last remaining physical dimension is mandatory, leading to the notion of now heavily researched SDM systems [91], [92], with the hope to get per-fiber capacities back onto a solid growth track, cf. Fig. 1(a).

#### F. Spectral Efficiency and Pulse Shaping

In our above considerations we were mostly concerned with constellation size and symbol rate. However, from Section II we know that the choice of analog transmit waveforms is another important aspect of digital communication signals. Traditionally, high-speed optical communication transmitters have used electronic multiplexers to generate binary drive signals, whose exact pulse shape is determined by the multiplexer's output stage and hence depends on the characteristics of the underlying high-speed electronics. Fig. 8(a) shows a typical electronic non-return-to-zero (NRZ) drive waveform, measured at 56 Gb/s. Note that high-speed electronic drive signals like this contain a significant amount of *non-linear ISI with memory*, i.e., they cannot generally be represented as a linearly filtered version of an ideal QAM signal according to (4). Hence, linear equalization cannot entirely remove ISI from signals based on such waveforms, which inherently results in an ISI-induced implementation penalty, even after linear equalization within the coherent receiver.

Starting with high-speed electronic drive waveforms, higher-order QAM signals can either be generated in the optical domain by means of parallel, binary-driven modulator structures [11], [40], or in the electrical domain by first synthesizing high-speed multi-level electrical drive signals that are then imprinted onto

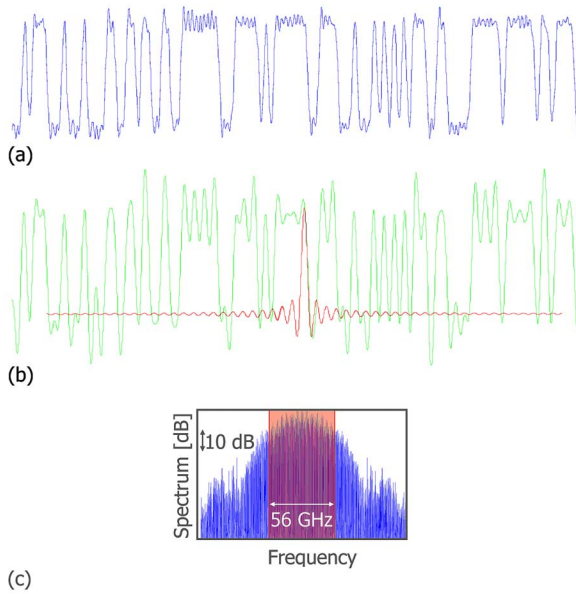


Fig. 8. (a) Electronically multiplexed measured 56-Gb/s NRZ waveform, (b) Ideal sinc pulse and corresponding waveform representing the same bit pattern, and (c) measured and ideal optical spectra.

the two quadratures of the optical field using an I/Q modulator [82]. Both methods generate optical signals whose analog pulse shapes contain non-linear ISI with memory and whose spectral shapes are determined by the characteristics of the electronics. Fig. 8(c) shows a typical resulting spectrum with its wide main lobe and its pronounced sidelobes. Both spectral features generate crosstalk among tightly spaced WDM channels and are hence of concern for high-spectral-efficiency systems. One partial mitigation option is the use of pre-modulation electronic filters or post-modulation optical filters to truncate the spectrum in an analog manner [82].

Recently, researchers have also applied ‘faster-than-Nyquist’ signaling [93], [94] by over-filtering the transmit signal, i.e., the transmit filter is chosen so narrow that it induces substantial (linear) ISI onto the transmit waveform [95], [96], [111]. While this technique allows WDM channels to be spaced closer together, the induced ISI needs to be compensated at the receiver by *sequence detection* (as opposed to the much simpler symbol-by-symbol detection) [33], such as maximum a-posteriori (MAP) detection or maximum likelihood sequence estimation (MLSE) [95], [96], [111]. This way, it is possible to transmit at spectral efficiencies exceeding the number of bits/symbol of the underlying modulation format, e.g., at sufficiently high received SNR one can transmit at or above 4 b/s/Hz using PDM-QPSK, as shown in Fig. 6(b). Note, however, that the same spectral efficiencies can be achieved by using richer symbol constellations at the transmitter and simpler symbol-by-symbol detection at the receiver. This leads to a trade-off between transmit constellation size, analog pulse shaping, and receive DSP complexity. Importantly, all techniques are upper-bounded by the corresponding Shannon capacity at the respective received SNR (cf. Fig. 6(b)).

Optimum spectral and temporal pulse shaping to generate ISI-free QAM signals is best done using an oversampled

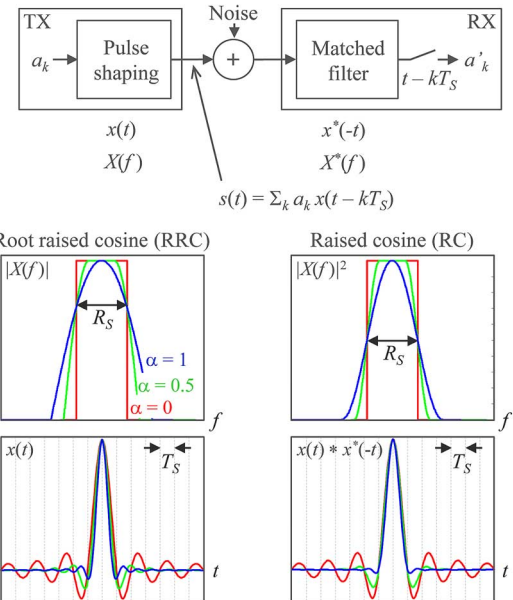


Fig. 9. The role of raised-cosine and square-root raised cosine pulses with  $\alpha = 0, 0.5, 1$  in a basic digital communication link according to (4).

transmit DAC that simultaneously performs the task of generating the QAM symbols and shaping the pulse waveform  $x(t)$  according to (4). To achieve ISI-free performance, as discussed in the context of signal orthogonality in Section II.B, it is well known in digital communications that pulse shapes meeting the Nyquist criterion need to be established at the sampling point within the receiver [33]. The most important class of Nyquist pulses has a *raised-cosine* (RC) shaped spectrum, where a shape parameter  $\alpha$  varies the roll-off from infinitely steep (rectangular spectrum,  $\alpha = 0$ ) to gradual (cosine-shaped spectrum,  $\alpha = 1$ ), as visualized in Fig. 9. The corresponding time-domain waveform for  $\alpha = 0$  has  $\sin(t)/t$  (‘sinc’) characteristics, with a long lasting oscillatory behavior; larger values of  $\alpha$  induce stronger damping and hence shorten the filter length needed to digitally shape the transmit pulses, albeit at the expense of a weaker spectral confinement. Note that the optimum receive filter in a digital communication link should match the transmitted pulse spectrum<sup>6</sup> (‘*matched filter*’) [33], which implies that *root raised cosine* (RRC) pulses  $x(t)$  should be transmitted, i.e., pulses whose spectrum  $X(f)$  is the square-root of a RC spectrum [33]. In fact, it is these pulses that obey the orthogonality relations of (3). While RRC pulses by themselves contain ISI, the matched receive filter produces  $X(f) \cdot X^*(f) = |X(f)|^2$  and hence turns RRC pulses back into ISI-free RC pulses (cf. Fig. 9).

Fig. 8(b) shows the waveform corresponding to the bit pattern of Fig. 8(a) but using sinc pulses (i.e., RRC pulses with  $\alpha = 0$ ). As can be seen by comparing the two waveforms in (a) and (b), the *peak-to-average power ratio* (PAPR) is increased when going from a standard binary drive waveform to RRC pulses. As with OFDM transmit waveforms, this increase in PAPR may pose practical problems, since the transmit DAC

<sup>6</sup>Strictly speaking, the aggregate filter function after the addition of white noise needs to be matched to the aggregate pulse shape prior to the addition of white noise for maximum SNR at the decision gate [33].

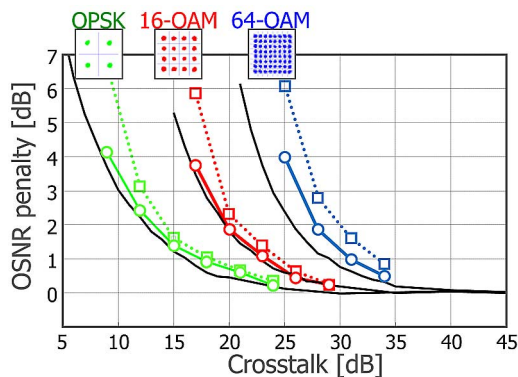


Fig. 10. Tolerance of various higher-order modulation formats to in-band crosstalk. (Solid curves: theory; circles and squares: experiments at 21.4 GBaud without and with CD, respectively) [110].

has to be able to faithfully generate the entire waveform without much amplitude clipping. Hence, a trade-off between spectral confinement, pulse shaping, filter impulse response length, PAPR, appropriately oversampled DAC resolution, and ultra-dense WDM or optical superchannel system performance has to be made [97], [98]. Nyquist pulse shaping forms the basis for many recent high-spectral-efficiency single-carrier and multi-carrier optical communication experiments [40], [72], [99]–[101]. Pulse shapes with increased tolerance to fiber nonlinearities are also being explored [102].

### G. Spectral Efficiency versus Crosstalk Tolerance

In addition to noise from optical amplifiers and linear and nonlinear distortions from fiber propagation and networking elements, signals in optical networks may suffer from crosstalk among neighboring WDM channels as well as from crosstalk originating from spurious signals within the same wavelength slot. The former, referred to as *WDM crosstalk* [97], [98], [103], results in trade-offs between spectral confinement (i.e., pulse shaping), permissible overheads for pilots and FEC, and WDM channel spacing. The latter, generally referred to as *in-band crosstalk*, may arise within multi-degree mesh ROADMs [104], [105], imperfect splices and connectors [106], or in the form of multi-path interference in Raman amplified systems [107], [108]. In-band crosstalk acts in a similar way as amplifier noise [87], [108]–[110], the difference being that it is not typically Gaussian distributed (but has the amplitude distribution of the underlying modulation) and is not typically white (but has the spectral shape of the signal itself). Hence, the tolerance of various higher-order modulation formats to crosstalk closely follows their tolerance to optical amplifier noise. Fig. 10 shows the crosstalk induced OSNR penalty at a BER of  $10^{-3}$  for (single-polarization) QPSK, 16-QAM, and 64-QAM [110]. The solid black curves represent a simple theoretical model, circles denote the case of an interferer having the same CD as the signal, and squares represent a substantially dispersed interferer (see [110] for details). Introducing dispersion onto the interferer slightly increases crosstalk penalties due to the larger PAPR of the dispersed interfering signal, resulting in larger peak excursions of the crosstalk induced perturbations

compared to a well-confined, undispersed interfering constellation. As the back-to-back implementation penalty in this 21.4-GBaud experiment increases from 0.9 dB (QPSK) to 1.8 dB (16-QAM) and 4.0 dB (64-QAM), the crosstalk tolerance also shrinks compared to theory. For a 1-dB crosstalk penalty, QPSK shows a tolerance of about 16 dB, while 64-QAM requires less than about 32 dB of crosstalk, which can become challenging in practical systems with multiple mesh ROADMs; the required 24 dB of crosstalk for 16-QAM is much more manageable in deployed networks. These considerations reveal yet another trade-off that limits the constellation size (and with it the spectral efficiency) in mesh networks, regardless of reach and delivered OSNR.

## IV. CONCLUSION

We have discussed the general structure of advanced optical modulation formats for digital coherent detection systems with respect to their *digital* (constellation) and *analog* (pulse shaping) properties. We have shown how symbol rate, constellation size, and pulse shaping impact the scaling of per-channel interface rates and WDM spectral efficiencies in various optical networking contexts. The resulting trade-offs, which include fundamental as well as technological components, point at 16-QAM as a promising sweet spot that represents a good compromise between various limiting effects but still enables high-speed, high-capacity long-haul optical networking.

## ACKNOWLEDGMENT

The author would like to thank S. Chandrasekhar, A. Chraplyvy, I. Dedic, R.-J. Essiambre, G. Foschini, A. Gnauck, S. Korotky, G. Kramer, A. Leven, X. Liu, T. Pfau, J. Sinsky, S. Randel, G. Raybon, R. Ryf, R. Tkach, and C. Xie for insightful discussions.

## REFERENCES

- [1] R. W. Tkach, "Scaling optical communications for the next decade and beyond," *Bell Labs Tech. J.*, vol. 14, no. 4, pp. 3–9, 2010.
- [2] S. K. Korotky, "Traffic trends: Drivers and measures of cost-effective and energy-efficient technologies and architectures for backbone optical networks," in *Opt. Fiber Commun. Conf.*, Los Angeles, CA, 2012, Paper OM2G.1.
- [3] M. A. Taubenblatt, "Optical interconnects for high-performance computing," *J. Lightw Technol.*, vol. 30, no. 4, pp. 448–457, Feb. 2012.
- [4] Y. A. Vlasov, "Silicon CMOS-integrated nano-photonics for computer and data communications beyond 100 G," *IEEE Commun. Mag.*, vol. 50, no. 2, pp. S67–S72, Feb. 2012.
- [5] J. Gray and P. Shenoy, "Rules of thumb in data engineering," Microsoft Res., Redmond, WA, Tech. Rep. MS-TR-99-100, 2000.
- [6] J. L. Hennessy and D. A. Patterson, *Computer Architectures: A Quantitative Approach*. San Francisco, CA: Morgan Kaufmann, 2003.
- [7] [Online]. Available: [http://www.top500.org/lists/2011/11/performance\\_development](http://www.top500.org/lists/2011/11/performance_development)
- [8] H. Kogelnik, "On optical communication: Reflections and perspectives," in *Proc. Eur. Conf. Opt. Commun.*, Stockholm, Sweden, 2004, Paper Mo1.1.1.
- [9] P. J. Winzer, "Beyond 100G Ethernet," *IEEE Commun. Mag.*, vol. 48, no. 7, pp. 26–30, Jul. 2010.
- [10] A. H. Gnauck *et al.*, "2.5 Tb/s (64 × 42.7 Gb/s) transmission over 40 × 100 km NZDSF using RZ-DPSK format and all-Raman-amplified spans," in *Proc. Opt. Fiber Commun. Conf.*, Anaheim, CA, 2002, Paper FC2.

- [11] R. A. Griffin and A. C. Carter, "Optical differential quadrature phase-shift key (oDQPSK) for high capacity optical transmission," in *Proc. Opt. Fiber Commun. Conf.*, Anaheim, CA, 2002, Paper WX6.
- [12] A. H. Gnauck and P. J. Winzer, "Optical phase-shift-keyed transmission," *J. Lightw. Technol.*, vol. 23, no. 1, pp. 115–130, Jan. 2005.
- [13] P. J. Winzer and R.-J. Essiambre, "Advanced optical modulation formats," *Proc. IEEE*, vol. 94, no. 5, pp. 952–985, May 2006.
- [14] D. A. Fishman *et al.*, "LambdaXtreme transport system: R&D of a high capacity system for low cost, ultra long haul DWDM transport," *Bell Labs Tech. J.*, vol. 11, no. 2, pp. 27–53, 2006.
- [15] A. Ohta *et al.*, "43-Gbps RZ-DQPSK transponder for long-haul optical transmission system," Yokogawa Tech. Report English Edition, No. 46, 2008.
- [16] P. J. Winzer *et al.*, "107-Gb/s optical ETDM transmitter for 100G Ethernet transport," in *Proc. Eur. Conf. Opt. Commun. Conf.*, Glasgow, U.K., 2005, Paper Th4.1.1.
- [17] G. Raybon *et al.*, "1-Tbit/s (10 × 107 Gbit/s) electronically multiplexed optical signal generation and WDM transmission," *J. Lightw. Technol.*, vol. 25, no. 1, pp. 233–238, Jan. 2007.
- [18] P. J. Winzer *et al.*, "100-Gb/s DQPSK transmission: From laboratory experiments to field trials," *J. Lightw. Technol.*, vol. 26, no. 20, pp. 3388–3402, Oct. 2008.
- [19] F. Derr, "Coherent optical QPSK intradyne system: Concept and digital receiver realization," *J. Lightw. Technol.*, vol. 10, no. 9, pp. 1290–1296, Sep. 1992.
- [20] M. G. Taylor, "Coherent detection method using DSP for demodulation of signal and subsequent equalization of propagation impairments," *IEEE Photon. Technol. Lett.*, vol. 16, no. 2, pp. 674–676, Feb. 2004.
- [21] R. Noe, "PLL-free synchronous QPSK polarization multiplex/diversity receiver concept with digital I&Q baseband processing," *IEEE Photon. Technol. Lett.*, vol. 17, no. 4, pp. 887–889, Apr. 2005.
- [22] D.-S. Lu-Gagnon *et al.*, "Coherent detection of optical quadrature phase-shift keying signals with carrier phase estimation," *J. Lightw. Technol.*, vol. 24, no. 1, pp. 12–21, Jan. 2006.
- [23] S. J. Savory *et al.*, "Digital equalization of 40 Gbit/s per wavelength transmission over 2480 km of standard fibre without optical dispersion compensation," in *Proc. Eur. Conf. Opt. Commun.*, Cannes, France, 2006, Paper Th2.5.5.
- [24] A. Leven *et al.*, "Real-time implementation of 4.4 Gbit/s QPSK intradyne receiver using field programmable gate array," *Electron. Lett.*, vol. 42, no. 24, pp. 1421–1422, Nov. 2006.
- [25] C. Laperle *et al.*, "Wavelength division multiplexing (WDM) and polarization mode dispersion (PMD) performance of a coherent 40 Gbit/s dual-polarization quadrature phase shift keying (DP-QPSK) transceiver," in *Proc. Opt. Fiber Commun. Conf.*, Anaheim, CA, 2007, Paper PDP16.
- [26] C. R. S. Fludger *et al.*, "Coherent equalization and POLMUX-RZ-DQPSK for robust 100-GE transmission," *J. Lightw. Technol.*, vol. 26, no. 1, pp. 64–72, Jan. 2008.
- [27] H. Sun *et al.*, "Real-time measurements of a 40 Gb/s coherent system," *Opt. Exp.*, vol. 16, pp. 873–879, 2008.
- [28] R.-J. Essiambre *et al.*, "Capacity limits of optical fiber networks," *J. Lightw. Technol.*, vol. 28, no. 4, pp. 662–701, Feb. 2010.
- [29] B. Zhu *et al.*, "112-Tb/s space-division multiplexed DWDM transmission with 14-b/s/Hz aggregate spectral efficiency over a 76.8-km seven-core fiber," *Opt. Exp.*, vol. 19, no. 17, pp. 16665–16671, 2011.
- [30] J. Sakaguchi *et al.*, "19-core fiber transmission of 19 × 100 × 172-Gb/s SDM-WDM-PDM-QPSK signals at 305 Tb/s," in *Proc. Opt. Fiber Commun. Conf.*, Los Angeles, CA, 2012, Paper PDP5C.1.
- [31] C. E. Shannon, "A mathematical theory of communication," *Bell Syst. Tech. J.*, vol. 27, pp. 379–423, 623–656, 1948.
- [32] P. J. Winzer and R.-J. Essiambre, "Evolution of digital optical modulation formats," in *Broadband Optical Modulators*, A. Chen and E. Murphy, Eds. Boca Raton, FL: CRC Press, 2012.
- [33] J. G. Proakis and M. Salehi, *Digital Communications*, 5th ed. New York: McGraw-Hill, 2007.
- [34] P. J. Winzer and R.-J. Essiambre, "Advanced optical modulation formats," in *Optical Fiber Telecommunications V-B: Systems and Networks*, I. P. Kaminov, T. Li, and A. E. Willner, Eds. Burlington, MA: Academic, 2008.
- [35] D. Marcuse, *Light Transmission Optics*. New York: Van Nostrand, 1972.
- [36] P. Tan and N. C. Beaulieu, "Analysis of the effects of Nyquist pulse-shaping on the performance of OFDM systems with carrier frequency offset," *Eur. Trans. Telecommun.*, vol. 20, pp. 9–22, 2009.
- [37] E. Agrell and M. Karlsson, "Power-efficient modulation formats in coherent transmission systems," *J. Lightw. Technol.*, vol. 27, no. 22, pp. 5115–5126, Nov. 2009.
- [38] M. Karlsson and E. Agrell, "Spectrally efficient four-dimensional modulation," in *Proc. Opt. Fiber Commun. Conf.*, Los Angeles, CA, 2012, Paper OTu2C.1.
- [39] X. Liu *et al.*, "Demonstration of record sensitivities in optically preamplified receivers by combining PDM-QPSK and M-ary pulse-position modulation," *J. Lightw. Technol.*, vol. 30, no. 4, pp. 406–413, Feb. 2012.
- [40] S. Chandrasekhar and X. Liu, "OFDM based superchannel transmission technology," *J. Lightw. Technol.*, vol. 30, no. 24, pp. 3816–3823, Dec. 2012.
- [41] G. Bosco *et al.*, "Performance limits of Nyquist-WDM and CO-OFDM in high-speed PM-QPSK systems," *IEEE Photon. Technol. Lett.*, vol. 22, no. 15, pp. 1129–1131, Aug. 2010.
- [42] W. Shieh and X. Chen, "Information spectral efficiency and launch power density limits due to fiber nonlinearity for coherent optical OFDM systems," *IEEE Photonics J.*, vol. 3, no. 2, pp. 158–173, Apr. 2011.
- [43] S. Kilmurray *et al.*, "Comparison of the nonlinear transmission performance of quasi-Nyquist WDM and reduced guard interval OFDM," *Opt. Exp.*, vol. 20, no. 4, pp. 4198–4205, 2012.
- [44] *ITU-T Recommendation G975.1*, Appendix I.9, 2004.
- [45] T. Mizuoichi *et al.*, "Evolution and status of forward error correction," in *Proc. Opt. Fiber Commun. Conf.*, Los Angeles, CA, 2012, Paper OTu2A.6.
- [46] F. Chang *et al.*, "Forward error correction for 100 G transport networks," *IEEE Commun. Mag.*, vol. 48, no. 3, pp. S48–S55, Mar. 2010.
- [47] G. D. Forney and G. Ungerboeck, "Modulation and coding for linear Gaussian channels," *IEEE Trans. Inf. Theory*, vol. 44, no. 6, pp. 2384–2415, Oct. 1998.
- [48] H. Bulow *et al.*, "Optical trellis-coded modulation (oTCM)," in *Proc. Opt. Fiber Commun. Conf.*, Los Angeles, CA, 2004, Paper WM5.
- [49] G. Kramer *et al.*, "Spectral efficiency of coded phase shift keying for fiber-optic communication," *J. Lightw. Technol.*, vol. 21, no. 10, pp. 2438–2445, Oct. 2003.
- [50] X. Liu *et al.*, "Transmission of 44-Gb/s coherent optical OFDM signal with trellis-coded 32-QAM subcarrier modulation," in *Proc. Opt. Fiber Commun. Conf.*, San Diego, CA, 2010, Paper OMR3.
- [51] M. Magarini *et al.*, "Concatenated coded modulation for optical communications systems," *IEEE Photon. Technol. Lett.*, vol. 22, no. 16, pp. 1244–1246, Aug. 2010.
- [52] H. Batshon *et al.*, "Ultra high speed optical transmission using sub-carrier-multiplexed four-dimensional LDPC coded modulation," *Opt. Exp.*, vol. 18, no. 19, pp. 20546–20551, 2010.
- [53] B. Sklar, *Digital Communications*, 2nd ed. Upper Saddle River, NJ: Prentice-Hall, 2001.
- [54] T. M. Cover and J. A. Thomas, *Elements of Information Theory*, 2nd ed. New York: Wiley, 2006.
- [55] J. R. Barry, E. A. Lee, and D. G. Messerschmitt, *Digital Communication*, 3rd ed. Norwell, MA: Kluwer, 2004.
- [56] X. Liu and S. Chandrasekhar, "Advanced modulation formats for core networks," in *Proc. Optoelectron. Commun. Conf.*, 2011, pp. 399–400.
- [57] T. Wang, G. Wellbrock, and O. Ishida, Eds., "Optical communications supplement next generation optical transport beyond 100G," *IEEE Commun. Mag.*, vol. 50, no. 2, pp. s2–s72, Feb. 2012.
- [58] I. Tomkos, B. Mukherjee, S. K. Korotky, R. S. Tucker, and L. Lunardi, Eds., "The evolution of optical networking," *Proc. IEEE*, vol. 100, no. 5, pp. 1017–1022, May 2012.
- [59] G. Raybon *et al.*, "All-ETDM 80-Gbaud (640-Gb/s) PDM 16-QAM generation and coherent detection," *IEEE Photon. Technol. Lett.*, vol. 24, no. 15, pp. 1328–1330, Aug. 2012.
- [60] Y. Kamio *et al.*, "Pre-equalization for 10 Gsymbol/s 16-QAM in a vector modulator," in *Proc. IEEE/LEOS Summer Top. Meet.*, 2008, Paper MC1.2.
- [61] [Online]. Available: <http://www.fujitsu.com/emea/services/microelectronics/dataconverters/chais>
- [62] M. Möller, "High-speed electronic circuits for 100 Gb/s transport networks," in *Proc. Opt. Fiber Commun. Conf.*, San Diego, CA, 2010, Paper OThC6.
- [63] T. Ellermeier *et al.*, "DA and AD converters in SiGe technology: Speed and resolution for ultra high data rate applications," in *Proc. Eur. Conf. Opt. Commun.*, Torino, Italy, 2010, Paper Th.10.A.6.

- [64] S. Chandrasekhar *et al.*, "Transmission of a 1.2-Tb/s 24-carrier no-guard-interval coherent OFDM superchannel over 7200-km of ultra-large-area fiber," in *Proc. Eur. Conf. Opt. Commun.*, 2009, pp. 1–2, Paper PD2.6.
- [65] F. A. Kish *et al.*, "Current status of large-scale InP photonic integrated circuits," *J. Sel. Topics Quantum Electron.*, vol. 17, no. 6, pp. 1470–1488, Nov.–Dec. 2011.
- [66] J. K. Fischer *et al.*, "Integrated coherent receiver modules for 100G Ethernet and beyond," in *Proc. Photon. Netw.*, 2011, pp. 1–5.
- [67] T. Pfau *et al.*, "Hardware-efficient coherent digital receiver concept with feedforward carrier recovery for M-QAM constellations," *J. Lightw. Technol.*, vol. 27, no. 8, pp. 989–999, Apr. 2009.
- [68] R. H. Walden, "Analog-to-digital converters and associated IC technologies," in *Proc. Compound Semicond. Integr. Circuits. Symp.*, 2008, pp. 1–2.
- [69] R. H. Walden, "Analog-to-digital converter survey and analysis," *IEEE J. Sel. Areas Commun.*, vol. 17, no. 4, pp. 539–550, Apr. 1999.
- [70] I. Dedic, "56Gs/s ADC : Enabling 100GbE," in *Proc. Opt. Fiber Commun. Conf.*, San Diego, CA, 2010, Paper OThT6.
- [71] Fujitsu Semiconductors Europe GmbH, Private Communication, 2012.
- [72] M. Nakazawa *et al.*, "Ultrafast coherent optical transmission," *J. Sel. Topics Quantum Electron.*, vol. 18, no. 1, pp. 363–376, Jan.–Feb. 2012.
- [73] Alcatel-Lucent 1830 Photonic Service Switch, Brochures and Data Sheets [Online]. Available: [www.alcatel-lucent.com](http://www.alcatel-lucent.com)
- [74] G. Agrawal, *Nonlinear Fiber Optics*, 4th ed. San Diego, CA: Elsevier, 2006.
- [75] S. J. Savory, "Digital filters for coherent optical receivers," *Opt. Exp.*, vol. 16, no. 2, pp. 804–817, 2008.
- [76] C. Xie, "Fiber nonlinearities in 16QAM transmission systems," in *Proc. 37th Eur. Conf. Opt. Commun.*, Geneva, Switzerland, 2011, Paper We.7.B.6.
- [77] E. Ip and J. M. Kahn, "Feedforward carrier recovery for coherent optical communications," *J. Lightw. Technol.*, vol. 25, no. 9, pp. 2675–1692, Sep. 2007.
- [78] M. G. Taylor, "Phase estimation methods for optical coherent detection using digital signal processing," *J. Lightw. Technol.*, vol. 27, no. 7, pp. 901–914, Apr. 2009.
- [79] S. Zhang *et al.*, "A performance investigation of adaptive phase estimations in coherent optical communications," *IEEE Photon Technol. Lett.*, vol. 23, no. 8, pp. 462–464, Apr. 2011.
- [80] D. Qian *et al.*, "101.7-Tb/s (370 × 294-Gb/s) PDM-128QAM-OFDM transmission over 3 × 55-km SSMF using pilot-based phase noise mitigation," in *Proc. Opt. Fiber Commun. Conf.*, Los Angeles, CA, 2011, Paper PDPB5.
- [81] A. H. Gnauck *et al.*, "Generation and transmission of 21.4-Gbaud PDM 64-QAM using a novel high-power DAC driving a single I/Q modulator," *J. Lightw. Technol.*, vol. 30, no. 4, pp. 532–536, Feb. 2012.
- [82] P. J. Winzer *et al.*, "Spectrally efficient long-haul optical networking using 112-Gb/s polarization-multiplexed 16-QAM," *J. Lightw. Technol.*, vol. 28, no. 4, pp. 547–556, Feb. 2010.
- [83] G. Raybon *et al.*, "All-ETDM 107-Gbaud (214-Gb/s) single-polarization QPSK transmitter and coherent receiver," in *Proc. Eur. Conf. Opt. Commun.*, Amsterdam, The Netherlands, 2012, Paper We.3.A.2.
- [84] W. Shieh and K.-P. Ho, "Equalization-enhanced phase noise for coherent detection systems using electronic digital signal processing," *Opt. Exp.*, vol. 16, no. 20, pp. 15718–15727, 2008.
- [85] C. Xie, "Local oscillator phase noise induced penalties in optical coherent detection systems using electronic chromatic dispersion compensation," in *Proc. Opt. Fiber Commun. Conf.*, San Diego, CA, 2009, Paper OMT4.
- [86] X. Liu *et al.*, "Generation and FEC-decoding of a 231.5-Gb/s PDM-OFDM signal with 256-iterative-polar-modulation achieving 11.15-b/s/Hz intrachannel spectral efficiency and 800-km reach," in *Proc. Opt. Fiber Commun. Conf.*, Los Angeles, CA, 2012, PDP5B.3.
- [87] J. Bromage, "Raman amplification for fiber communications systems," *J. Lightw. Technol.*, vol. 22, no. 1, pp. 79–93, Jan. 2004.
- [88] E. Ip and J. M. Kahn, "Fiber impairment compensation using coherent detection and digital signal processing," *J. Lightw. Technol.*, vol. 28, no. 4, pp. 502–519, Feb. 2010.
- [89] P. J. Winzer, "Energy-efficient optical transport capacity scaling through spatial multiplexing," *IEEE Photon. Technol. Lett.*, vol. 23, no. 13, pp. 851–853, Jul. 2011.
- [90] R.-J. Essiambre and R. W. Tkach, "Capacity trends and limits of optical communication networks," *Proc. IEEE*, vol. 100, no. 5, pp. 1035–1055, May 2012.
- [91] T. Morioka *et al.*, "Enhancing optical communications with brand new fibers," *IEEE Commun. Mag.*, vol. 50, no. 2, pp. s31–s42, Feb. 2012.
- [92] P. J. Winzer, "Optical networking beyond WDM," *IEEE Photon. J.*, vol. 4, no. 2, pp. 647–651, Apr. 2012.
- [93] J. E. Mazo, "Faster-than-Nyquist signaling," *Bell Syst. Tech. J.*, vol. 54, no. 8, pp. 1451–1462, 1975.
- [94] G. Colavolpe, "Faster-than-Nyquist and beyond: How to improve spectral efficiency by accepting interference," in *Proc. Eur. Conf. Opt. Commun.*, Geneva, Switzerland, 2011, Paper Mo1.B.1.
- [95] J.-X. Cai *et al.*, "20 Tbit/s transmission over 6860 km with sub-Nyquist channel spacing," *J. Lightw. Technol.*, vol. 30, no. 4, pp. 651–657, Feb. 2012.
- [96] Y. Cai *et al.*, "High spectral efficiency long-haul transmission with pre-filtering and maximum a posteriori probability detection," in *Proc. 35th Eur. Conf. Opt. Commun.*, Torino, Italy, 2010, Paper We.7.C.4.
- [97] G. Bosco *et al.*, "On the performance of Nyquist-WDM Terabit superchannels based on PM-BPSK, PM-QPSK, PM-8QAM or PM-16QAM subcarriers," *J. Lightw. Technol.*, vol. 29, no. 1, pp. 53–61, Jan. 2011.
- [98] J. Wang *et al.*, "Generation of spectrally efficient Nyquist-WDM QPSK signals using digital FIR or FDE filters at transmitters," *J. Lightw. Technol.*, to be published.
- [99] X. Zhou *et al.*, "PDM-Nyquist-32QAM for 450-Gb/s per-channel WDM transmission on the 50 GHz ITU-T Grid," *J. Lightw. Technol.*, vol. 30, no. 4, pp. 553–559, Feb. 2012.
- [100] A. Sano *et al.*, "102.3-Tb/s (224 × 548-Gb/s) C- and extended L-band all-Raman transmission over 240 km using PDM-64QAM single carrier FDM with digital pilot tone," in *Proc. Opt. Fiber Commun. Conf.*, Los Angeles, CA, 2012, Paper PDP5.C3.
- [101] S. Randel *et al.*, "Generation of 224-Gb/s multicarrier offset-QAM using a real-time transmitter," in *Proc. Opt. Fiber Commun. Conf.*, Los Angeles, CA, 2012, Paper OM2H.2.
- [102] B. Chatelain *et al.*, "Optimized pulse shaping for intra-channel nonlinearities mitigation in a 10 Gbaud dual-polarization 16-QAM system," in *Proc. Opt. Fiber Commun. Conf.*, Los Angeles, CA, 2012, 2011, Paper OW05.
- [103] P. J. Winzer *et al.*, "Coherent crosstalk in ultradense WDM systems," *J. Lightw. Technol.*, vol. 23, no. 4, pp. 1734–1744, Apr. 2005.
- [104] S. Tibuleac and M. Filer, "Transmission impairments in DWDM networks with reconfigurable optical add-drop multiplexers," *J. Lightw. Technol.*, vol. 28, no. 4, pp. 557–567, Feb. 2010.
- [105] S. Gringeri *et al.*, "Flexible architectures for optical transport nodes and networks," *IEEE Commun. Mag.*, vol. 48, no. 7, pp. 40–50, Jul. 2010.
- [106] A. D. Yablon, *Optical Fiber Fusion Splicing*. New York: Springer-Verlag, 2005.
- [107] R.-J. Essiambre *et al.*, "Design of bidirectionally-pumped fiber amplifiers generating ASE and double Rayleigh backscattering at constant fiber Kerr nonlinearity," *IEEE Photon. Technol. Lett.*, vol. 14, no. 7, pp. 914–916, Jul. 2002.
- [108] J. Bromage *et al.*, "Multiple-path interference and its impact on system design," in *Raman Amplifiers and Oscillators in Telecommunications*, M. N. Islam, Ed. New York: Springer-Verlag, 2003.
- [109] J. Bromage *et al.*, "Relative impact of multiple-path interference and amplified spontaneous emission noise on optical receiver performance," in *Proc. Opt. Fiber Commun. Conf.*, Anaheim, CA, 2002, Paper TuR3.
- [110] P. J. Winzer *et al.*, "Penalties from in-band crosstalk for advanced optical modulation formats," in *Proc. Eur. Conf. Opt. Commun.*, Geneva, Switzerland, 2011, Paper Tu.5.B.7.
- [111] N. Alic, E. Myslivets, and S. Radic, "Non-coherent high spectral efficiency long haul waveband transmission," *IEEE Photon. Technol. Lett.*, vol. 24, no. 2, pp. 113–115, Jan. 2012.
- [112] H. Takara *et al.*, "1.01-Pb/s (12 SDM/222 WDM/456 Gb/s) crosstalk-managed transmission with 91.4-b/s/Hz aggregate spectral efficiency," in *Proc. Eur. Conf. Opt. Commun.*, Amsterdam, The Netherlands, Paper Th.3.C.1.

Author biography not included by author request due to space constraints.